Journal of Sound and Vibration (2001) **246**(3), 441–460
doi:10.1006/jsvi.2001.3573, available online at http://www.idealibrary.com on IDEAL®

IDENTIFICATION OF BOLTED JOINTS THROUGH LASER VIBROMETRY

X. MA

Department of Mechanical & Industrial Engineering, University of Illinois at Urbana-Champaign, Urbana, IL 61801, *U.S.A. E-mail: xma@uiuc.edu*

L. BERGMAN

Department of Aeronautical & Astronautical Engineering, University of Illinois at Urbana-Champaign, Urbana, IL 61801, *U.S.A. E-mail: lbergman@uiuc.edu*

AND

A. VAKAKIS

Department of Mechanical & Industrial Engineering, University of Illinois at Urbana-Champaign, Urbana, IL 61801, *U.S.A. E-mail: avakakis@uiuc.edu*

(*Received* 12 *November* 1999, *and in final form* 8 *January* 2001)

We present a new technique for identifying the dynamics of bolted joints. The technique relies on the comparison of the overall dynamics of the bolted structure to that of a similar but unbolted one. The difference in the dynamics of the two systems can be attributed solely to the joint; modelling this difference in the dynamics enables us to construct a non-parametric model for the joint dynamics. Non-contacting, laser vibrometry is utilized to experimentally measure the structural responses with increased accuracy and to perform scans of the structural modes at fixed frequency. A numerical algorithm is then developed to post-process the experimental data and identify the joint force. Theoretical calculations are first used to validate the technique, which is then utilized to identify a practical joint. Experimental force–displacement plots at the joint reveal clear hysteresis loops which, in turn, can be used to estimate the damping dissipation at the joint. Moreover, experimental frequency responses and scans of the mode shapes of the bolted structure reveal non-proportional damping and non-linear effects due to microimpacts of the connected beams at the bolted joint.

1. INTRODUCTION

The aim of this work is to create accurate computational models of bolted joints. These models should account for the linear as well as non-linear effects introduced by the bolted joints to the ambient structure. Such non-linear effects include microimpacts between the bolted structural elements, micro/macroslip, friction and hysteresis. The derived models should be in a form that makes them directly implementable in finite element codes.

Previous work on bolted joints was focused on characterizing slip damping and micro/macroslip [1, 2], on linear/non-linear damping effects and hysteresis [3, 4], [5–11], on system identification of joints [12–14], and on the dynamics and control structures with joints [15–18].

0022-460X/01/380441 + 20 $35.00/0

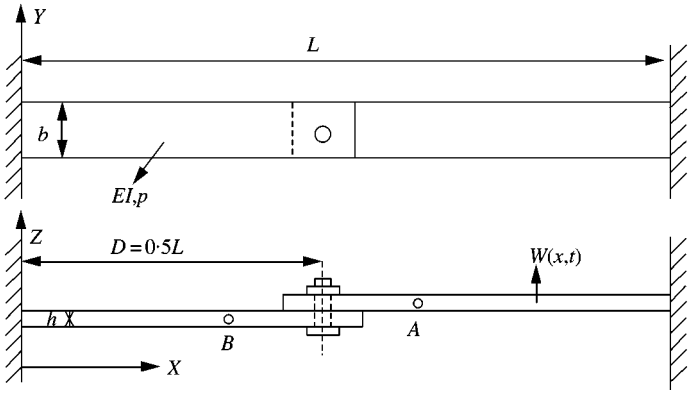

Figure 1. The beam structure with bolted joint.

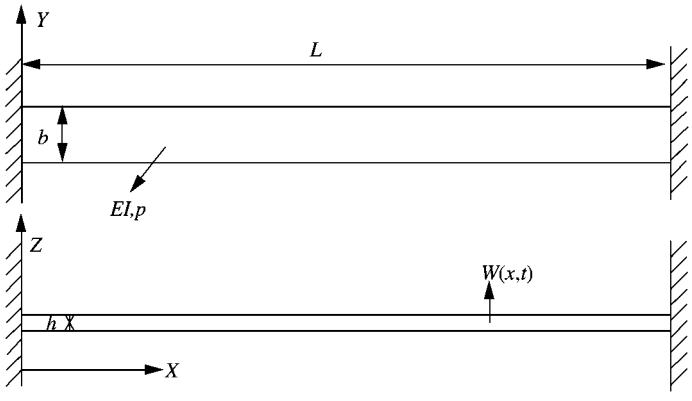

Figure 2. The uniform beam structure.

2. METHODOLOGY

The bolted structure considered in this work is shown in Figure 1. It includes two identical linear Euler/Bernoulli cantilever beams connected at their free ends by a bolted joint. Although this system has a relatively simple geometry, the methodology developed herein is applicable to bolted structures of more complex configurations. Depending on the amount of tightness in the joint, one expects to obtain non-linear dynamical effects due to (a) dry friction at the area of contact of the beams leading to hysteresis loops in the force–displacement plots, (b) micro/macroslip of the beams at their jointed parts that also leads to hysteresis phenomena, and (c) microimpacts due to the looseness of the joint. Such non-linear effects can drastically affect the dynamics of the bolted structure, and the proposed identification methodology must be capable of modelling them accurately.

The basic idea in the proposed methodology is to compare the dynamics of the bolted structure (labeled *Structure I*, *S-I*) with the dynamics of a linear uniform structure (labeled *Structure II*, *S-II*). S-II has the same dimensions and material properties as S-I but is composed of a *single* uniform beam with both ends clamped, without a joint (cf. Figure 2). Since the only structural difference between S-I and S-II is the bolted joint, it is logical to conclude that, *under identical forcing conditions, the difference in the dynamics between the*

two systems is solely due to the bolted joint effects. Hence, by carefully analyzing the difference in the dynamics between the two systems we should be able to accurately model the dynamics of the joint.

2.1. THEORETICAL MODELS

Considering S-I and S-II, we assume that the dynamics of the two systems can be reconciled by adding to S-II a *local* force operator $N(w(D, t), \dot{w}(D, t))\,\delta(x - D)$, which locally models the dynamical effects of the joint in S-I. Then, the dynamics of S-I are theoretically governed by the equation of motion

$$EIw''''(x, t) + \rho A\ddot{w}(x, t) + N(w(D, t), \dot{w}(D, t))\delta(x - D) = f(x, t) \text{ on } 0 < x < L, \tag{1}$$

where EI is the elasticity-moment of inertia distribution of the beam, ρ and A are the mass density per unit length and cross-sectional area, respectively, and $f(x, t)$ is the external force distribution. Primes denote partial differentiation with respect to x, whereas dots are with respect to t. We assume zero initial conditions.

In order to non-dimensionalize, we introduce the new variables

$$\bar{x} = x/L, \quad \bar{t} = \Omega t, \quad \Omega^2 = EI/\rho AL^4, \quad \bar{w} = w/L$$

and substitute these into equation (1) to obtain the non-dimensionalized equation

$$\bar{w}'''' + \ddot{\bar{w}} + \frac{L^2}{EI} N(\bar{w}(\bar{D}, \bar{t}), \dot{\bar{w}}(\bar{D}, \bar{t}))\bar{\delta}(\bar{x} - \bar{D}) = \frac{L^3}{EI} f(\bar{x}, \bar{t})$$

$$\Rightarrow \bar{w}'''' + \ddot{\bar{w}} + \bar{N}(\bar{w}(\bar{D}, \bar{t}), \dot{\bar{w}}(\bar{D}, \bar{t}))\bar{\delta}(\bar{x} - \bar{D}) = \bar{f}(\bar{x}, \bar{t}) \text{ on } 0 < \bar{x} < 1, \tag{2}$$

where $\bar{N}$ and $\bar{f}$ are non-dimensionalized variables.

In the absence of the joint, the dynamics of S-II are governed by the equation

$$\bar{w}'''' + \ddot{\bar{w}} = \bar{f}(\bar{x}, \bar{t}) \text{ on } 0 < \bar{x} < 1. \tag{3}$$

In the following analysis, the overbars will be omitted for simplicity. It is well known that the solution to linear system (3) can be expressed in the form

$$w \equiv w^{S\text{-}II}(x, t) = \int_{-\infty}^{t} \mathrm{d}\tau \int_0^1 g(x, \eta, t - \tau) f(\eta, \tau)\,\mathrm{d}\eta, \tag{4}$$

where the Green function is defined as

$$g(x, \eta, t) = \sum_{n=1}^{\infty} \mathrm{e}^{-\zeta_n \omega_n t} \frac{\phi_n(x)\phi_n(\eta)}{\omega_{dn}} \sin(\omega_{dn} t),$$

where $\phi_n(x)$ is the mass-normalized nth linear normal mode of S-II satisfying the condition

$$\int_0^1 \phi_n(x)\phi_m(x) = \delta_{nm}, \quad \delta_{nm} = \begin{cases} 1, & n = m, \\ 0, & n \neq m. \end{cases}$$

ζ_n is the nth critical damping ratio, ω_n is the nth undamped natural frequency and ω_{dn} is the nth damped natural frequency. In writing the above expression for the Green function we

assumed that S-II is proportionally damped, so that the undamped modeshapes are identical to the damped ones.

Returning now to the non-linear problem (2) (modelling the system with the bolted joint), we consider a harmonic external excitation $F\sin(\omega t)$ applied at position $x = \xi$ on the beam. We also regard the operator $N(w(D, t), \dot{w}(D, t))\delta(x - D)$ as a pseudo-force and place it to the right-hand side of the equation

$$w'''' + \ddot{w} = F\sin(\omega t)\delta(x - \xi) - N(w(D, t), \dot{w}(D, t))\delta(x - D). \tag{5}$$

Then the solution of the non-linear system is expressed as

$$w \equiv w^{S\text{-}I}(x, t) = \int_0^t \int_0^1 \left[\sum_{n=1}^{\infty} \mathrm{e}^{-\zeta_u \omega_u (t-\tau)} \frac{\phi_n(x)\phi_n(\eta)}{\omega_{dn}} \sin(\omega_{du}(t - \tau)) \right] [F\sin(\omega\tau)\delta(\eta - \xi)$$

$$- N(w(D, \tau), \dot{w}(D, \tau))\delta(\eta - D)]\,\mathrm{d}\eta\,\mathrm{d}\tau \tag{6}$$

or

$$w^{S\text{-}I}(x, t) = \int_0^t \int_0^1 g(x, \eta, t - \tau)\,[F\sin(\omega\tau)\delta(\eta - \xi)]\,\mathrm{d}\eta\,\mathrm{d}\tau$$

$$+ \int_0^t \int_0^1 g(x, \eta, t - \tau)[- N(w(D, \tau), \dot{w}(D, \tau))\delta(\eta - D)]\,\mathrm{d}\eta\,\mathrm{d}\tau. \tag{7}$$

Taking into account equation (4), we rewrite equation (7) as

$$w^{S\text{-}I}(x, t) = w^{S\text{-}II}(x, t) - \int_0^t g(x, D, t - \tau)N(w(D, \tau), \dot{w}(D, \tau))\,\mathrm{d}\tau. \tag{8}$$

Equation (8) is used to perform the system identification of the bolted joint. Indeed, the quantities $w^{S\text{-}I}(x, t)$ and $w^{S\text{-}II}(x, t)$ can be directly measured through laser vibrometry. In addition, the Green function in the kernel of the above integral can be theoretically computed using the previous series formula

$$g(x, \eta, t) = \sum_{n=1}^{\infty} \mathrm{e}^{-\zeta_n \omega_n t} \frac{\phi_n(x)\phi_n(\eta)}{\omega_{dn}} \sin(\omega_{dn} t), \tag{9}$$

where the summation is truncated to a sufficient number of terms, and $\phi_n(x)$, ζ_n, ω_n and ω_{dn} of S-II are experimentally estimated by means of modal analysis carried out on mobility frequency response functions measured through laser vibrometry. In the performed experiments the OMETRON VT 4010 laser vibrometer was used.

Once $w^{S\text{-}I}(x, t)$, $w^{S\text{-}II}(x, t)$ and $g(x, \eta, t)$ are computed, the operator N characterizing the dynamics of the joint can be accurately estimated through a discretization process. This will be discussed in the next section. We note that equation (8) holds for periodic as well as non-periodic forcing, although in the previous analysis we considered the case of harmonic excitation. Also, a basic assumption of the outlined methodology is that the dynamic effect of the joint is treated as a local (concentrated) effect. This assumption, however, can be relaxed by assuming a distributed joint dynamic effect, in which case equation (8) must be

replaced by the relation

$$w^{S\text{-}II}(x,t) = w^{S\text{-}I}(x,t) - \int_0^t \int_0^1 g(x,\eta,t-\tau) N(w(\eta,\tau),\dot{w}(\eta,\tau))[\mathrm{H}(L_2/L) - \mathrm{H}(L_1/L)]\,\mathrm{d}\eta\,\mathrm{d}\tau, \tag{10}$$

where H( ) is the Heaviside function and L_1 and L_2 define the domain of the bolted joint. However, in the present work, only expression (8) is utilized.

2.2. DISCRETIZATION SCHEME

To estimate the local dynamic effect of the joint, equation (8) is rewritten as

$$G(x,t) = w^{S\text{-}II}(x,t) - w^{S\text{-}I}(x,t) = \int_0^t g(x,D,t-\tau)P(\tau)\,\mathrm{d}\tau, \tag{11}$$

where $P(\tau) \equiv N(w(D,\tau),\dot{w}(D,\tau))$ is the joint force to be computed. At this point we fix x (the measurement point on S-I and S-II), and allow t to vary from 0 to T (the time window of the experimental measurement). In addition, we discretize the time variable according to $t_i = i\Delta t,\ i = 0,\ldots,n$, and discretize the integral in equation (11) by replacing it with a summation and restricting the variable τ to discrete values τ_i. Equation (11) is then expressible as

$$\begin{aligned} G(x,t_i) &= \sum_{k=0}^{i} g(x,D,t_i-\tau_k)\,P(\tau_k)\Delta t \\ &\Rightarrow G(x,\ t_i) = g(x,D,t_i-\tau_0)\Delta t P(\tau_0) + g(x,D,t_i-\tau_1)\Delta t P(\tau_1) + \cdots \\ &+ g(x,D,t_i-\tau_{i-1})\Delta t P(\tau_{i-1}) \quad i = 1,\ldots,n. \end{aligned} \tag{12}$$

Equation (12) can be written in matrix form as

$$\begin{Bmatrix} G(x,t_1)/\Delta t \\ \vdots \\ G(x,t_i)/\Delta t \\ \vdots \\ \vdots \\ G(x,t_n)/\Delta t \end{Bmatrix} =$$

$$\begin{bmatrix} g(x,D,t_1-\tau_0) & 0 & \cdots & 0 & \cdots & 0 \\ \vdots & \vdots & \vdots & \vdots & \vdots & \vdots \\ g(x,D,t_i-\tau_0) & \cdots & \cdots & g(x,D,t_i-\tau_{i-1}) & \cdots & 0 \\ \vdots & \vdots & \vdots & \vdots & \vdots & \vdots \\ \vdots & \vdots & \vdots & \vdots & \vdots & \vdots \\ g(x,D,t_n-\tau_0) & \cdots & \cdots & g(x,D,t_n-\tau_{i-1}) & \cdots & g(x,D,t_n-\tau_{n-1}) \end{bmatrix} \times \begin{Bmatrix} P(\tau_0) \\ \vdots \\ P(\tau_i) \\ \vdots \\ \vdots \\ P(\tau_{n-1}) \end{Bmatrix} \tag{13a}$$

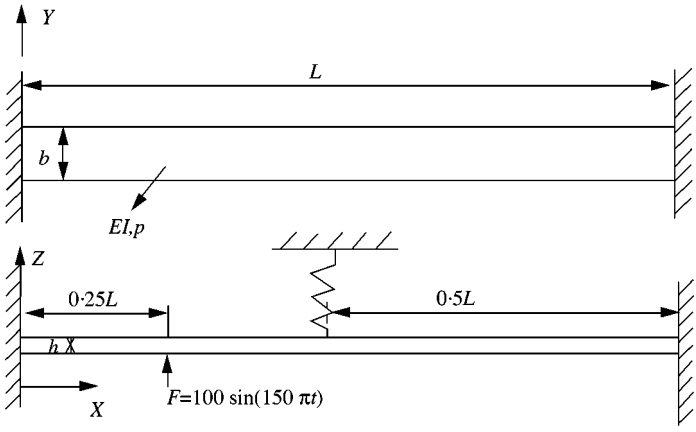

Figure 3. The beam-spring model for testing the analytical model.

or more compactly as

$$\{G\} = [g]\{P\}. \tag{13b}$$

Provided that matrix $[g]$ is non-singular (this condition is met in our case), the estimated time history of the local force due to the bolted joint can be computed by inverting equation (13):

$$\{P\} = [g]^{-1}\{G\}. \tag{14}$$

The fact that matrix $[g]$ is well behaved can be concluded by studying its structure from relation (13a). Indeed, since the Green function decays for sufficiently large time, the diagonal or near-diagonal terms of $[g]$ dominate over the non-diagonal terms. This feature enhances the numerical stability of the inverse matrix operation in equation (14).

The above computation completes the numerical estimation of the force due to the joint. Once equation (14) is completed, a plot of force versus displacement at the joint can be constructed numerically, and non-linear effects can be readily studied. In the following sections we provide theoretical validation of the proposed method and applications to experimental data.

3. APPLICATIONS TO THEORETICAL AND EXPERIMENTAL DATA

3.1. THEORETICAL VALIDATION

In order to validate the previous computational methodology, we first applied it to theoretical data resulting from numerical simulations of an undamped beam clamped at its ends and supported by a spring at its midpoint (cf. Figure 3). The spring generated the simulated 'joint' force to be identified. Two sets of numerical data were constructed, corresponding to beams with and without springs (with and without 'joints') respectively. A harmonic force was applied to the beams as shown in Figure 3. The simulations were performed by direct computation of truncated modal superposition series consisting of 10 terms (modes). Theoretical eigenfunctions and natural frequencies were employed. The simulations were then used to identify the force at the 'joint' by means of relation (14).

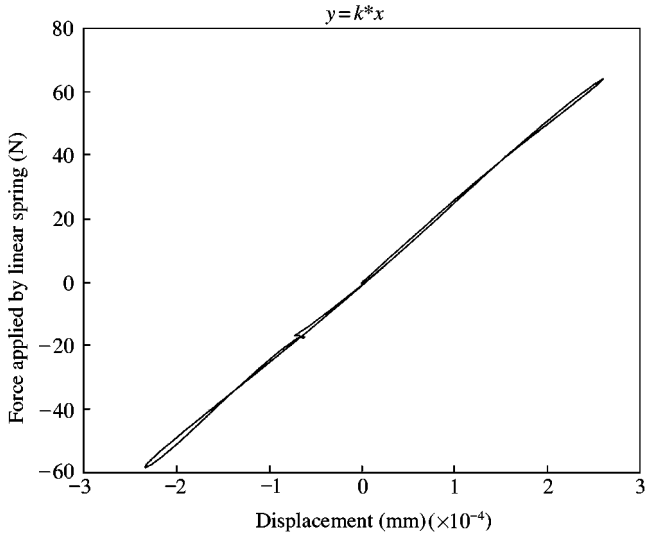

Figure 4. The load–displacement curve for the beam-linear spring model, from numerical simulation.

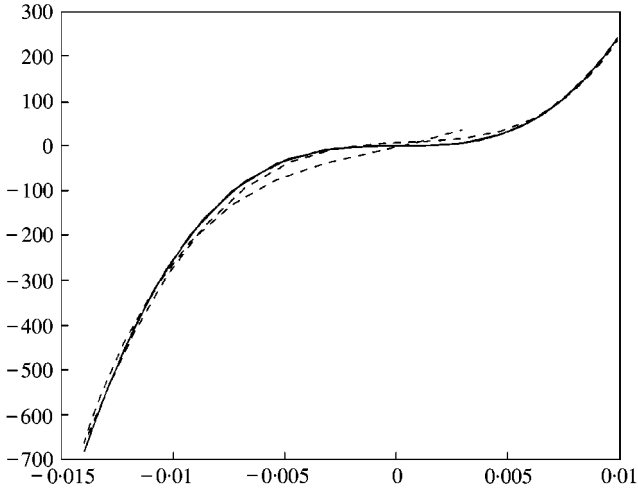

Figure 5. The load–displacement curve for the beam-non-linear spring model, from numerical simulation (——) and from the discretization scheme (- - - - -).

In Figure 4, the identified load–displacement curve for a 'joint' simulated by a linear spring with stiffness characteristic $P = 2{\cdot}5 \times 10^5 x$ is depicted. A similar calculation for a 'joint' simulated by a non-linear spring $P = 2{\cdot}5 \times 10^8 x^3$ is depicted in Figure 5. Satisfactory agreement between the theoretical and identified 'joint' forces is observed, validating the proposed identification methodology. The method was then used to identify the joint of the experimental fixture.

3.2. IDENTIFICATION OF THE EXPERIMENTAL BOLTED JOINT

The experimental bolted joint coupling two identical cantilever beams is pictured in Figure 6. The structural parameters of the beams are given by $EI = 53{\cdot}083\ \mathrm{Nm}^2$,

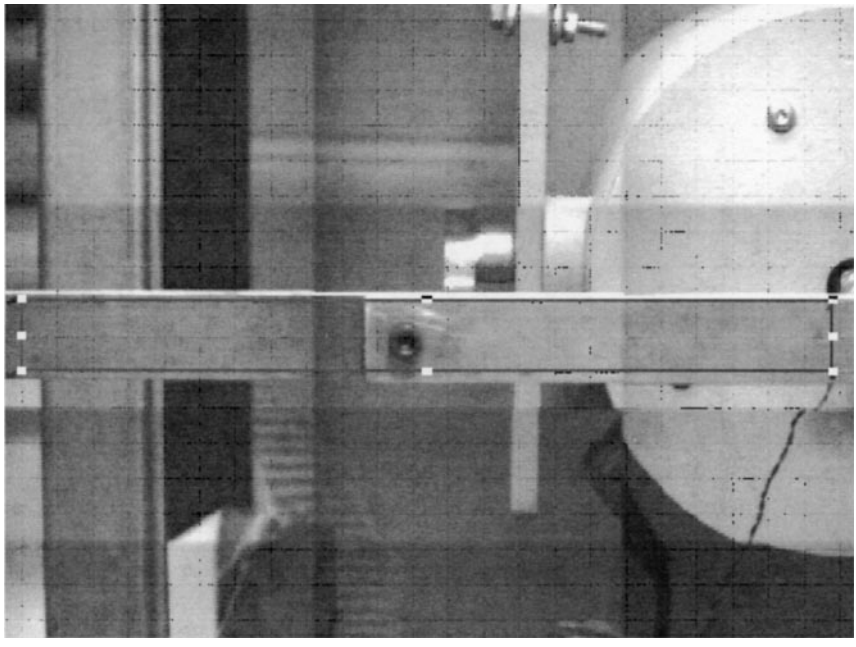

Figure 6. Photograph of actual test area on the beam.

$m = 0{\cdot}9825$ kg/m, $L = 0{\cdot}51$ m, $b = 0{\cdot}025$ m (width), and $h = 0{\cdot}005$ m (thickness). A concentrated external force was applied by means of an electromagnetic shaker through a stinger shaft at position $x = 0{\cdot}405$ m (cf. Figure 6). The transverse displacements of the beams were measured by non-contacting laser vibrometry, utilizing the OMETRON VT 4010 Laser Vibrometer. This piece of instrumentation enabled us to obtain interference-free measurements in the following two modes of operation: (a) mobility (velocity versus force) frequency response functions (FRFs) at isolated points of the structure; and (b) velocity r.m.s. scans at a single frequency over a selected area of the structure. The laser vibrometer possesses its own signal generator enabling sine sweep, transient or random modal tests, and its own modal analysis software for fast post-processing of the measured data.

We performed experiments with both S-I (with joint) and S-II (without joint). Regarding S-I, we differentiated between three levels of joint tightness: joint tightened by a torque of 10 ft lb (labeled S-Ia); a hand-tight joint (S-Ib); and a loose joint (S-Ic). The reasons for considering these three levels of joint tightness include: (a) to compare the dynamics of S-II (no joint) and S-Ia (a very tight joint); (b) to investigate non-linear effects due to weak (system S-Ib) and strong (system S-Ic) vibro-impacts on the dynamics; and (c) to investigate how loosening the joint affects the damping/non-linear forces generated through friction and micro/macroslip.

In Figures 7 and 8 we depict experimental velocity–frequency plots for the four systems, S-Ia,b,c and S-II, measured at positions A and B on the beams. These results were obtained by performing frequency sweeps from 0 to 1 kHz, while keeping the nominal level of the applied force at the fixed level 0·759 lb. Since the dynamics of S-I were non-linear, only velocity–frequency plots corresponding to the fixed level of input force were considered. In the measurement range 0–1 kHz there exist four modes of S-II, at frequencies 85 Hz (mode 1), 192·5 Hz (mode 2), 402·5 Hz (mode 3) and 747·5 Hz (mode 4) respectively. The non-linear variations of these resonance frequencies for S-Ia,b,c are depicted in Figure 9, where it is seen that the joint non-linearity has a softening effect on modes 1, 2, and 3.

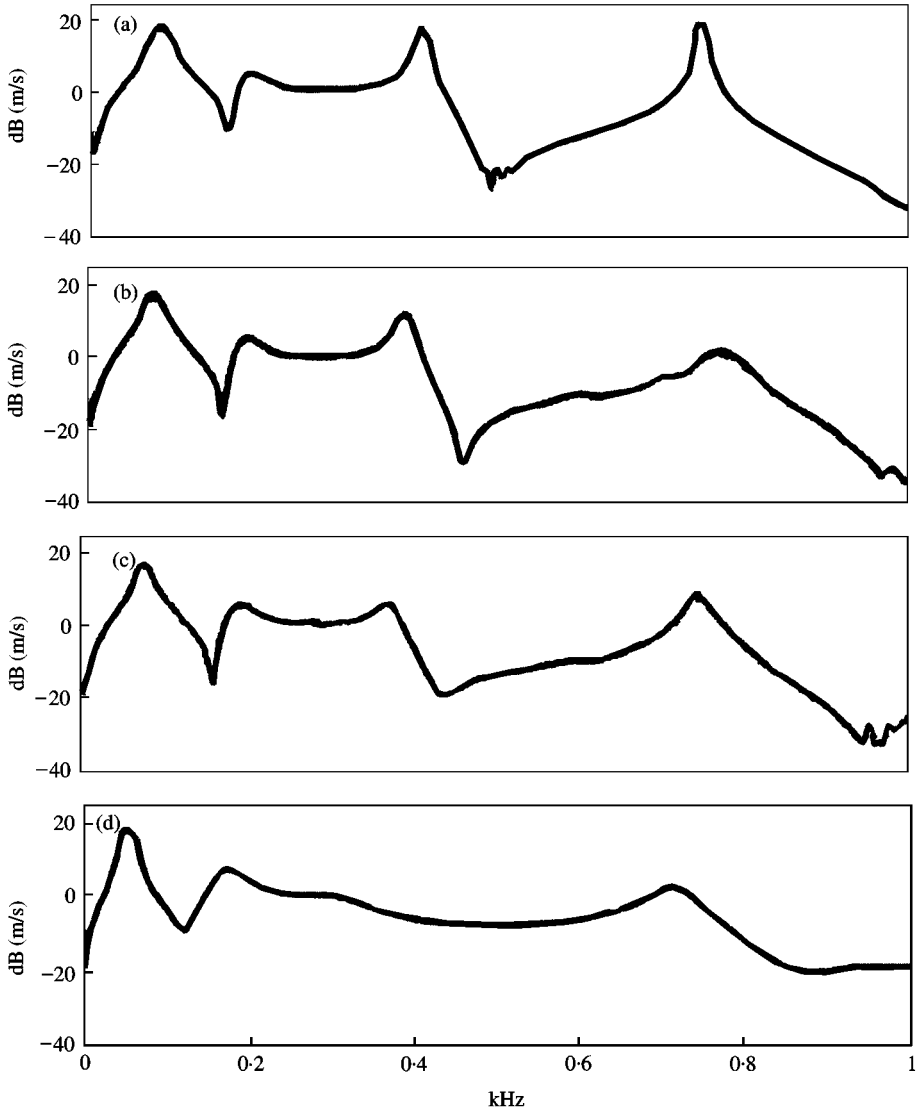

Figure 7. Mobility frequency response functions (FRFs) at point A of (a) S-II, (b) S-Ia, (c) S-Ib, and (d) S-Ic, by swept sine test using the laser vibrometer.

Regarding mode 4, we observe an interesting 'mode splitting' for S-Ia at measurement position B, and little variation of the resonance frequency for S-Ia,b at measurement position A. The effects of the joint non-linearity are evident in the velocity plots of S-Ic, where vibroimpacts of the beams due to the loose joint connection drastically affect the transverse responses.

The vibration shapes of the beams at selected frequencies were obtained by means of laser scans. The spatial distributions of the r.m.s. velocity amplitudes for the four systems are depicted in Figures 10 (75 Hz), 12 (187·5 Hz), 14 (370 Hz) and 16 (745 Hz). The spatial distributions of the corresponding steady state velocity phases are depicted in Figures 11, 13, 15 and 17 respectively. These four frequencies corresponded to resonances of S-Ib, and all the scans were performed there for comparison purposes. Moreover, the magnitude of

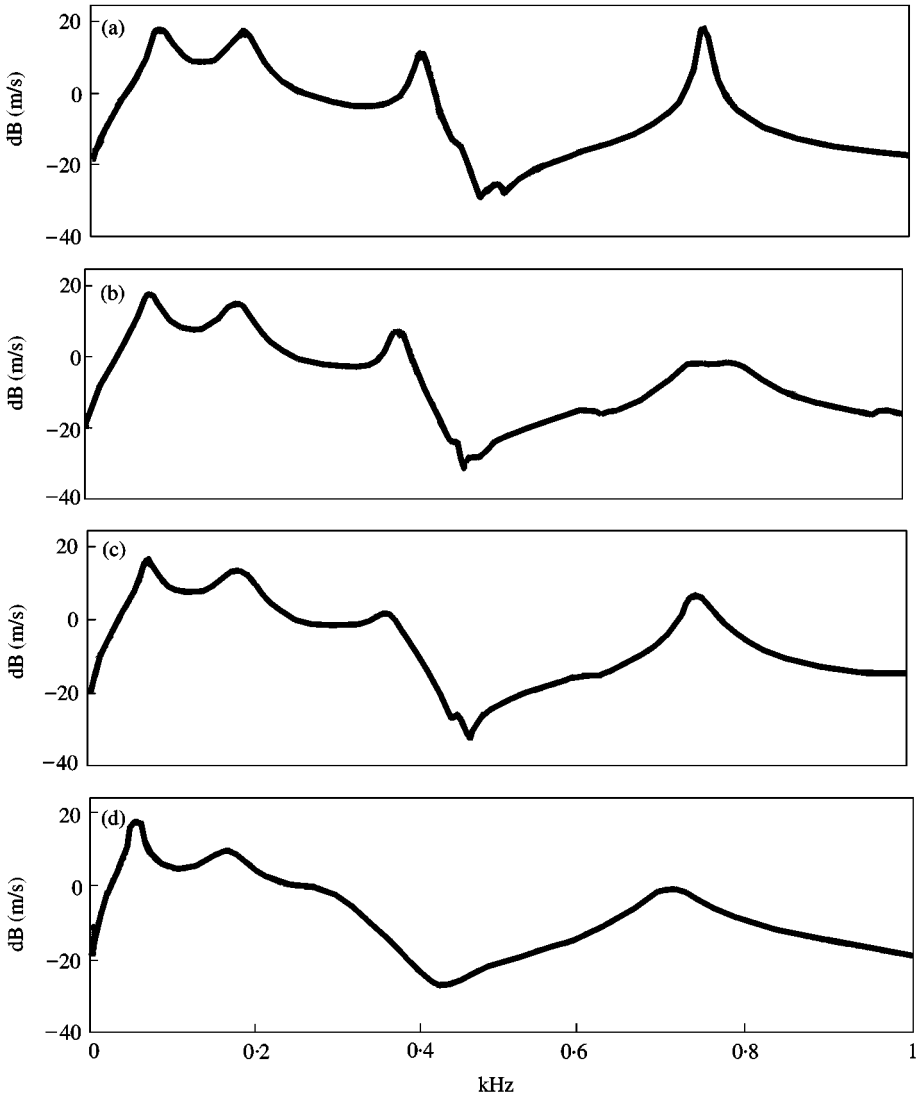

Figure 8. Mobility frequency response functions (FRFs) at point B of (a) S-II, (b) S-Ia, (c) S-Ib, and (d) S-Ic, by swept sine test using the laser vibrometer.

the applied shaker force for all scans was independently recorded in order to ensure that it was kept constant at the fixed levels 0·19 lb, 0·664 lb, 0·474 lb, 0·759 lb respectively. Considering the mode shapes of S-II, they correspond to bending modes with increasing number of nodal points as frequency increases. Mode 1 (Figures 10 and 11) does not appear to be greatly affected by the presence of the joint and corresponds to a 'breathing'-type standing wave. Mode 2 (Figures 12 and 13) possesses a single nodal point, which moves to the left as joint tightness decreases. More interestingly, we observe non-trivial phase values for S-Ib,c indicating mode complexities; we conjecture that these mode complexities are due either to the localized damping provided by the joint which renders the overall damping distribution of the system non-proportional, or to the joint non-linearities. The mode complexities become more evident in the modeshapes of mode 3 (Figures 14 and 15) with

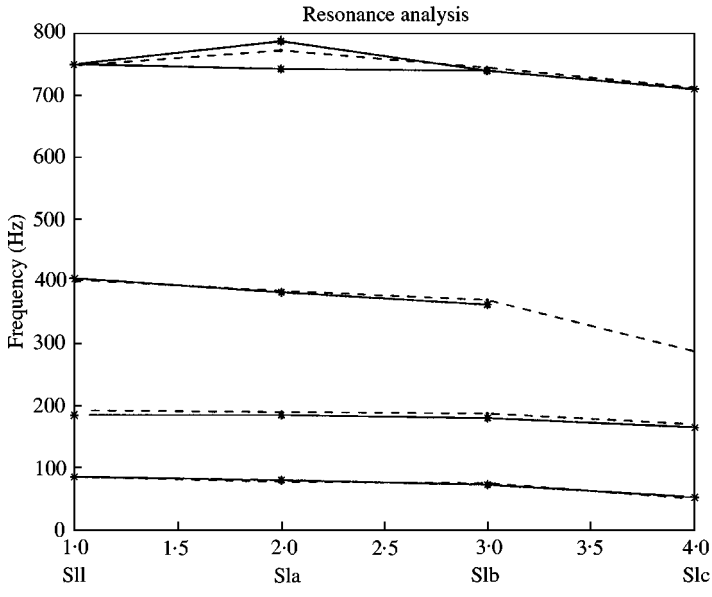

Figure 9. Resonant peaks of S-II, S-Ia,b,c (——) from FRFs at point A, (- - - - -) from FRFs at point B.

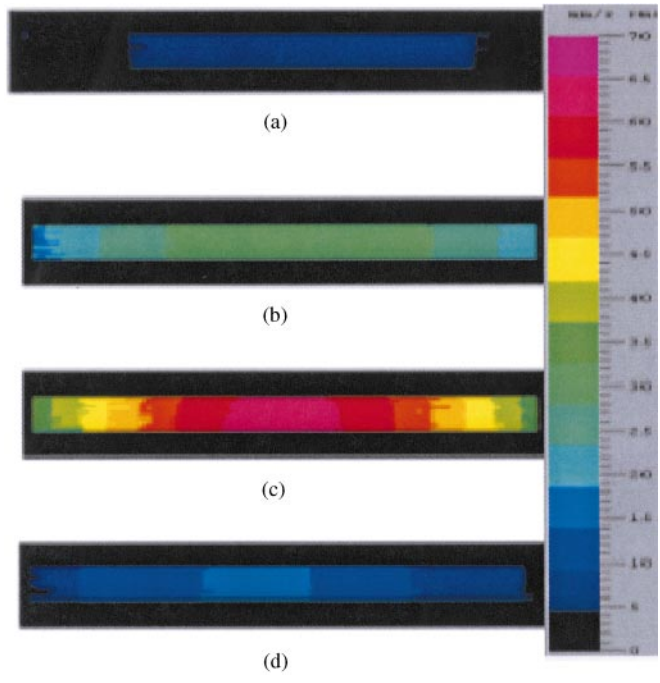

Figure 10. Velocity spatial distributions (r.m.s.) obtained by laser scans of the four beam configurations of (a) S-II, (b) S-Ia, (c) S-Ib, and (d) S-Ic at 75 Hz.

two nodal points. We note the torsional-like motion of the modeshape of S-Ic, caused by the looseness of the joint, that permits relative rotation of the tips of the two beams coupled at the joint. The torsional-type motion of S-Ic is more clear for mode 4 (Figures 16 and 17). In addition, mode complexities are more evident for this mode.

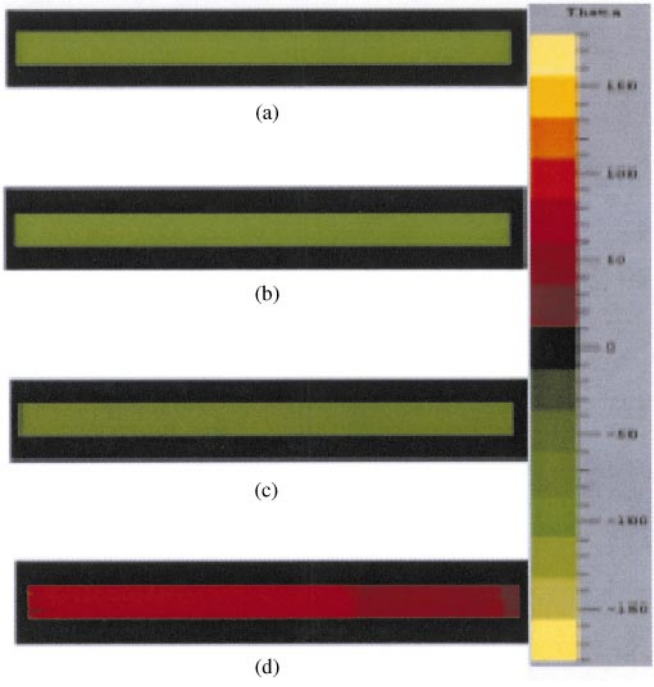

Figure 11. Phase plots obtained by laser scans of the four beam configurations of (a) S-II, (b) S-Ia, (c) S-Ib, and (d) S-Ic at 75 Hz.

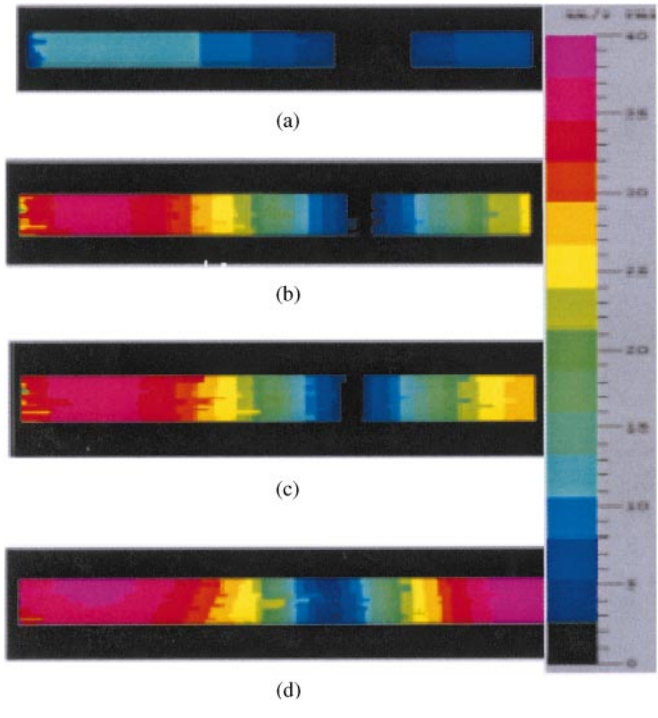

Figure 12. Velocity spatial distributions (r.m.s.) obtained by laser scans of the four beam configurations of (a) S-II, (b) S-Ia, (c) S-Ib, and (d) S-Ic at 187·5 Hz.

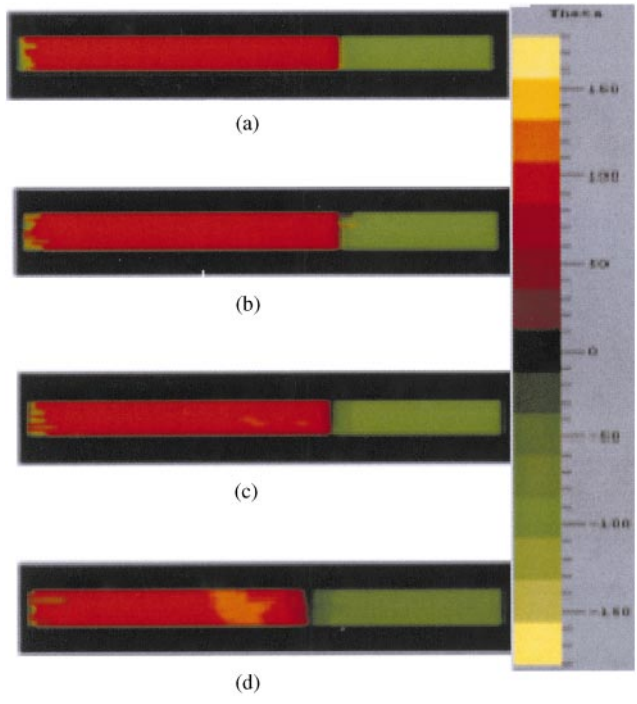

Figure 13. Phase plots obtained by laser scans of the four beam configurations of (a) S-II, (b) S-Ia, (c) S-Ib, and (d) S-Ic at 187·5 Hz.

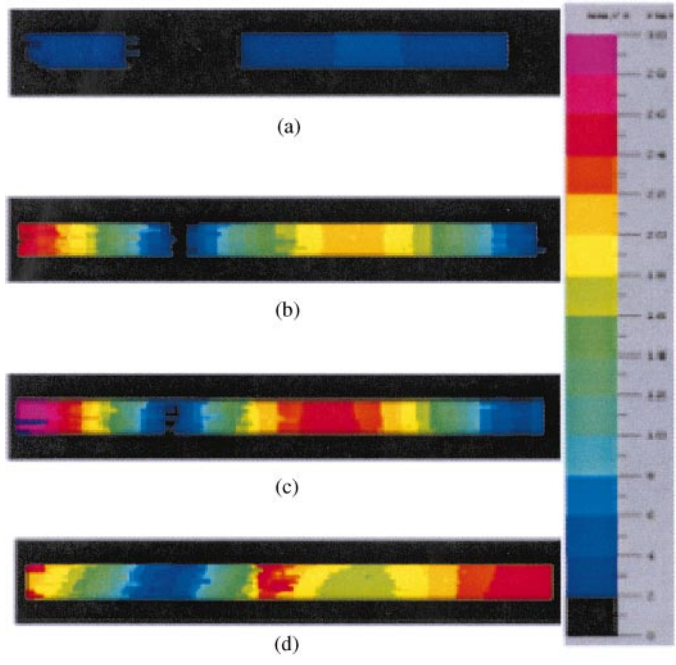

Figure 14. Velocity spatial distributions (r.m.s.) obtained by laser scans of the four beam configurations of (a) S-II, (b) S-Ia, (c) S-Ib, and (d) S-Ic at 370 Hz.

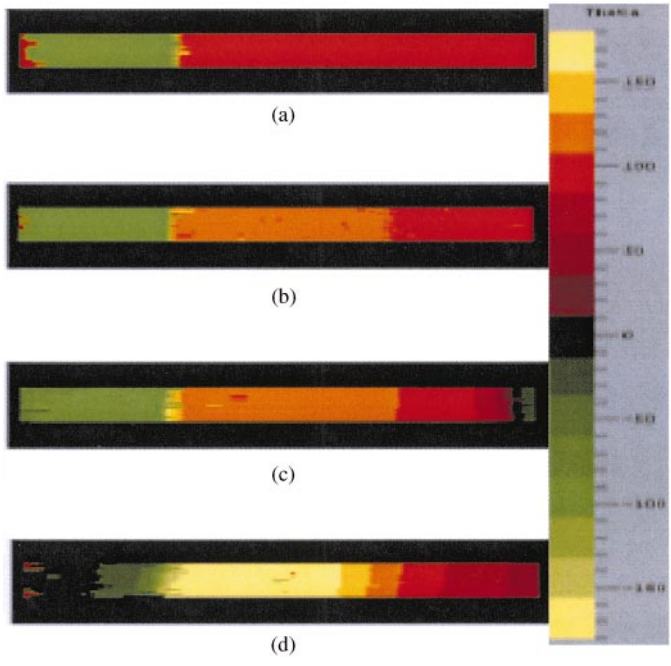

Figure 15. Phase plots obtained by laser scans of the four beam configurations of (a) S-II, (b) S-Ia, (c) S-Ib, and (d) S-Ic at 370 Hz.

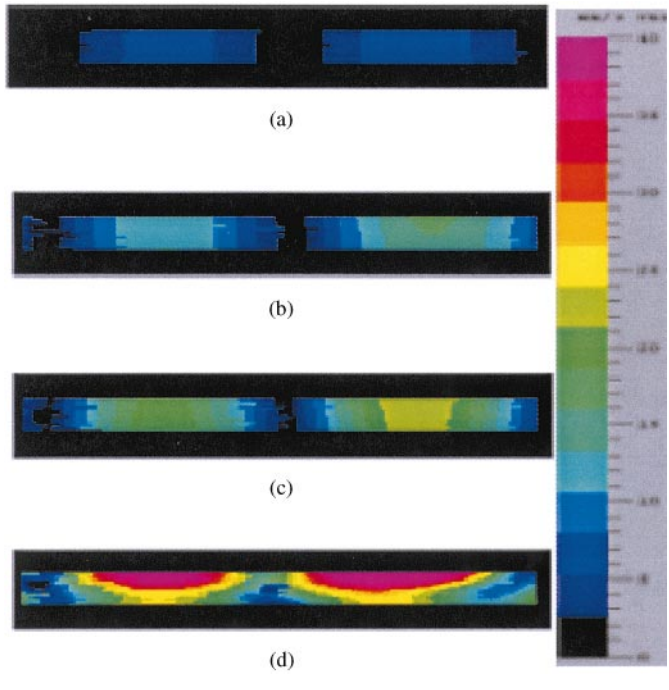

Figure 16. Velocity spatial distributions (r.m.s.) obtained by laser scans of the four beam configurations of (a) S-II, (b) S-Ia, (c) S-Ib, and (d) S-Ic at 745 Hz.

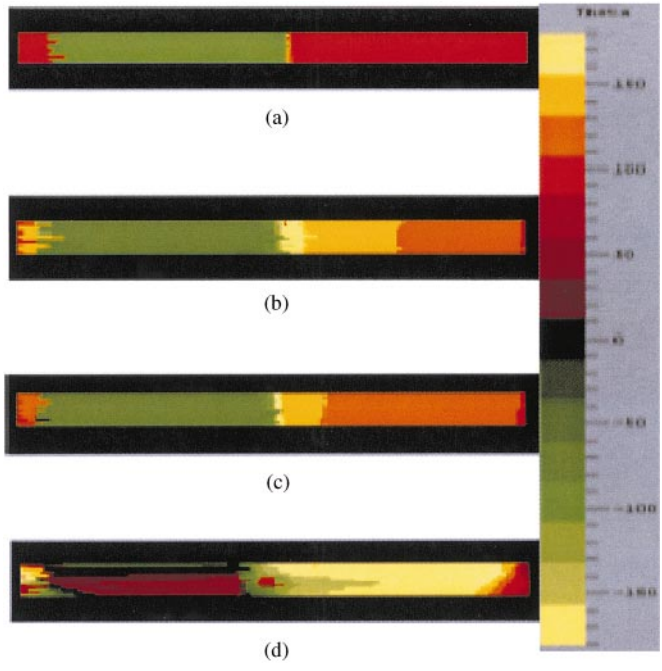

Figure 17. Phase plots obtained by laser scans of the four beam configurations of (a) S-II, (b) S-Ia, (c) S-Ib, and (d) S-Ic at 745 Hz.

Experimental measurements of transverse displacements were conducted to identify the joint force using the methodology described previously. In order to improve the accuracy of the estimation, we experimentally measured the mode shapes $\phi_n(x)$, damped natural frequencies ω_{dn} and viscous damping ratios ζ_n of S-II that are required for the computation of the Green function $g(x, \eta, t)$ in equation (14); this was performed by direct laser scans of the entire length of the beam at the natural frequency of the mode. The first six modeshapes of S-II are depicted in Figure 18.

In Figure 19, we depict the identified force–displacement relation for S-Ia at 370 Hz. An external harmonic force of magnitude 0·474 lb was used to excite the system through the shaker. In the same figure we present the time series for the measured transverse displacement at the joint and the identified force using equation (14). From the identified force–displacement plot, we note a clear hysteresis loop caused by the damping of the joint. In Figure 20 we present the force–displacement loops at the joint at various frequencies and for various systems. In particular, the hysteresis loops at 75 Hz (at a force magnitude of 0·19 lb) for S-Ia (Figure 20(a)), 760 Hz (0·759 lb) for S-Ia (Figure 20(b)), 745 Hz (0·759 lb) for S-Ib (Figure 20(c)) and 745 Hz (0·759 lb) for S-Ic. For S-Ia (very tight bolt) we note a nearly unperturbed hysteresis loop, whereas for the loosely joined structures S-Ib and S-Ic the hysteresis loop appears to be 'drifting' due to non-linear micro-vibro-impact effects.

We repeated the calculation with a transient force loading. This appears in Figure 21(a). The transient decaying joint displacement as well as the decaying identified force due to the joint are depicted in Figure 21(b). In Figure 21(c) we depict the force–displacement relation for the joint. This plot was developed by filtering out the high-frequency noise evidenced in the identified joint force plot of Figure 21(b). In this case, due to the transient nature of the external force, no clear hysteresis loops are formed.

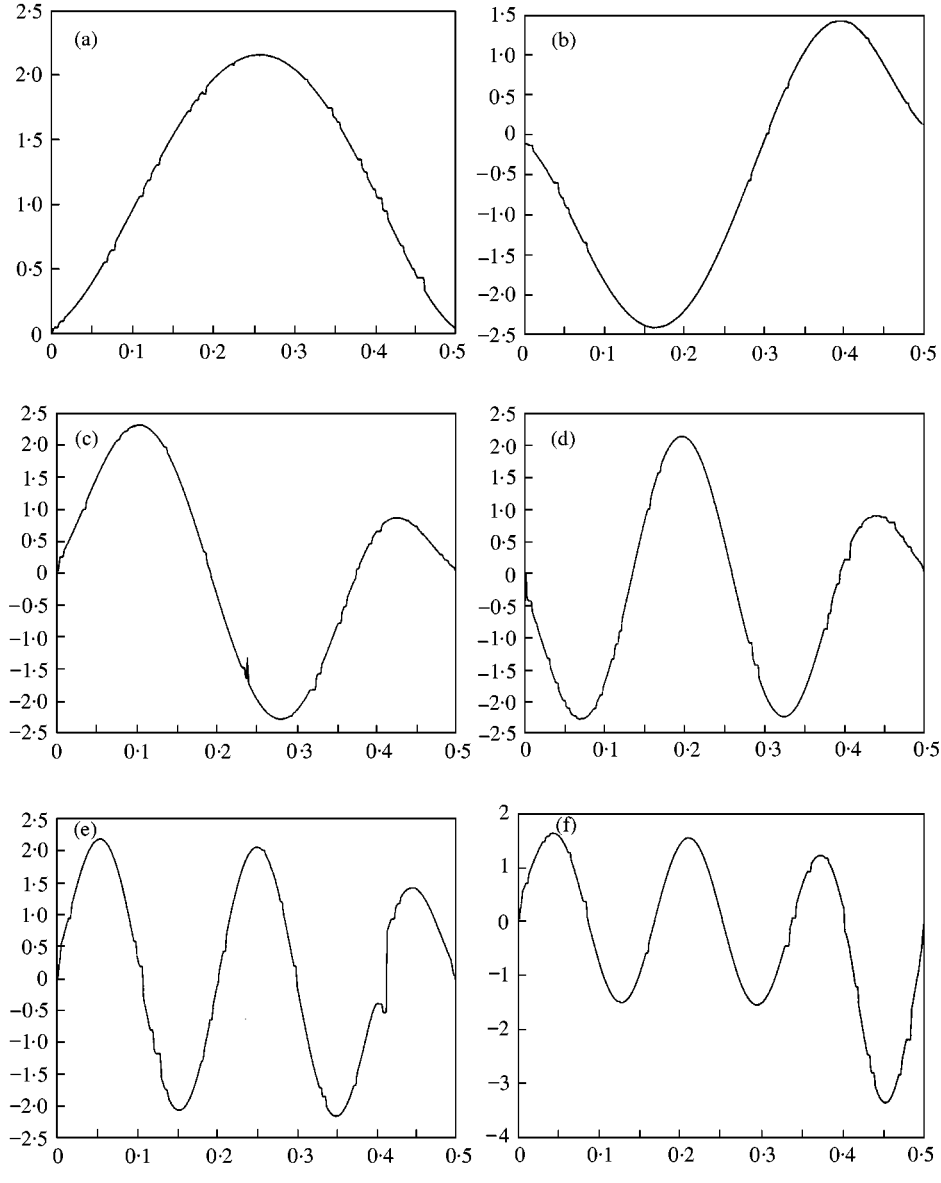

Figure 18. Experimentally derived normal modes of the uniform beam S-II, (a)–(f) are the normal modes 1–6.

4. CONCLUDING REMARKS

We have developed a system identification methodology to study the dynamic effects of a bolted joint. The method relies on comparing the dynamics of the ambient structure with and without the bolted joint, and on laser vibrometry to obtain interference-free, non-contacting vibration measurements. The basic features of the method are its relative simplicity and its applicability to a wide class of bolted structures (see comment (1) below).

There are various research paths through which this work can be extended. These include:

(1) Application of the proposed methodology to bolted structures of more complex configurations and geometries (frames, multiple beam connections). Single or multiple

bolted joints can be handled. A similar approach to the one followed herein can be employed; i.e., comparing the dynamics of the bolted structure to that of a uniform beam structure with no joint. The difference in the dynamics can be used to model the dynamic effects of the joint(s).

(2) Non-local modelling of the dynamic effect of the joint can be attempted by means of equation (10). This will enable one to compute a distributed dynamic joint effect by identifying the distributed force operator $N(w(\eta, \tau), \dot{w}(\eta, \tau))$. A discretization scheme similar to the one used in this work can be employed towards this goal.

(3) Independent modelling of the dynamics of each of the two bolted beams, and coupling of the two beam equations at the joint. This will provide us with a more sophisticated

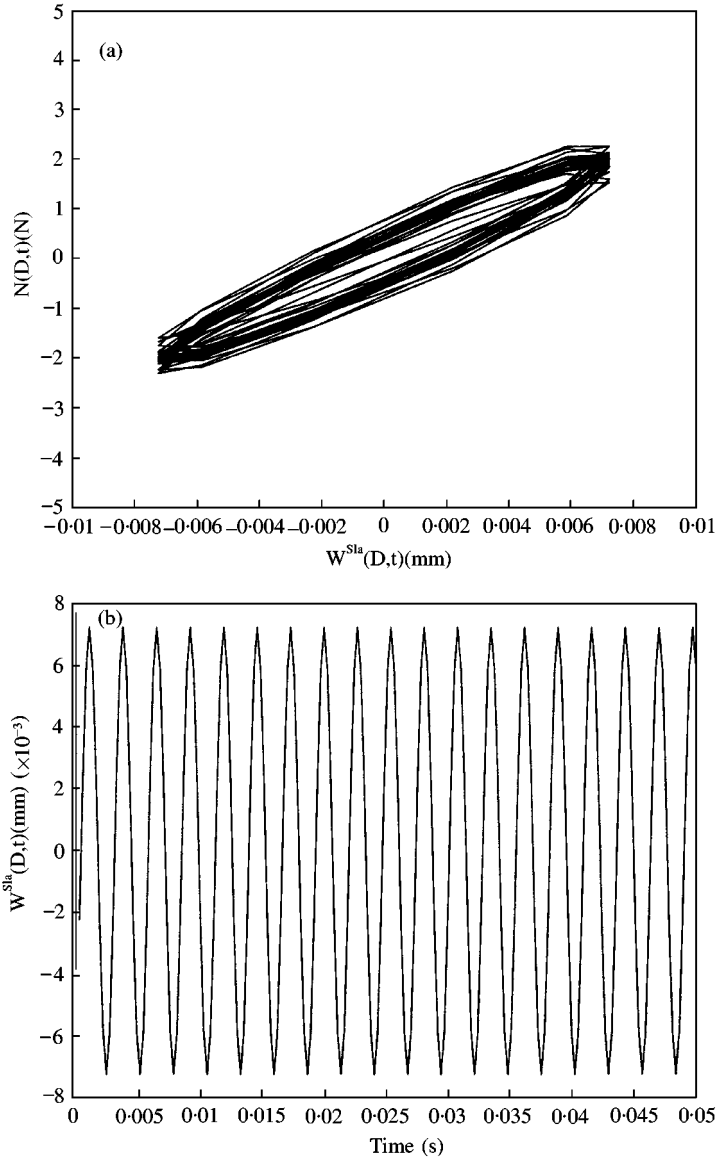

Figure 19. Harmonic response of beam S-Ia with input of 0·474 lb at 370 Hz. (a) Plot of force versus transverse displacement at the joint. (b) Plot of displacement versus time. (c) Plot of computed joint force versus time.

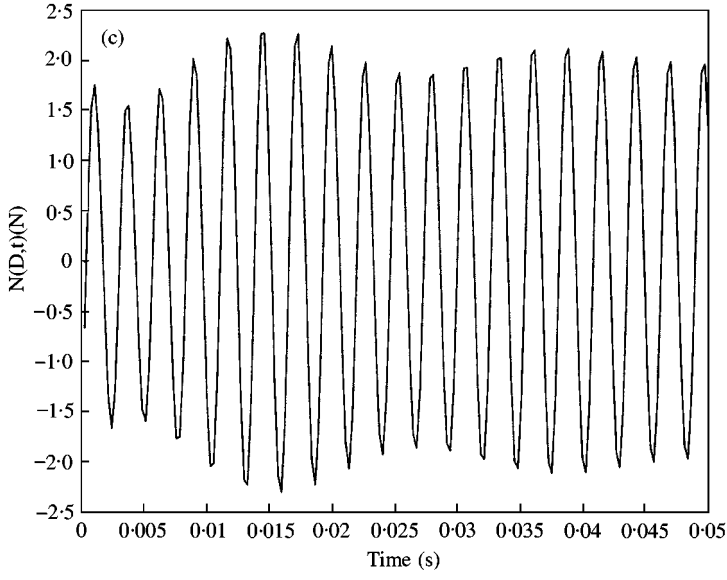

Figure 19. Continued.

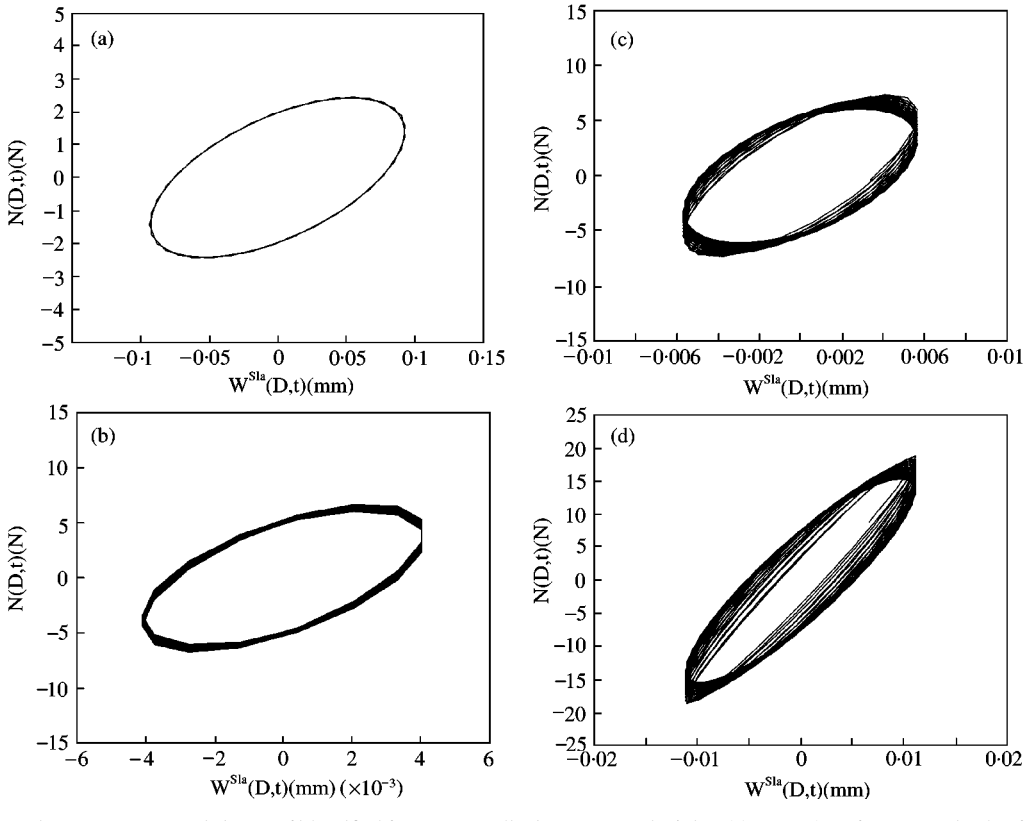

Figure 20. Hysteresis loops of identified force versus displacement at the joint: (a) 75 Hz (at a force magnitude of 0·19 lb) for S-Ia; (b) 760 Hz (0·759 lb) for S-Ia; (c) 745 Hz (0·759 lb) for S-Ib; (d) 745 Hz (0·759 lb) for S-Ic.

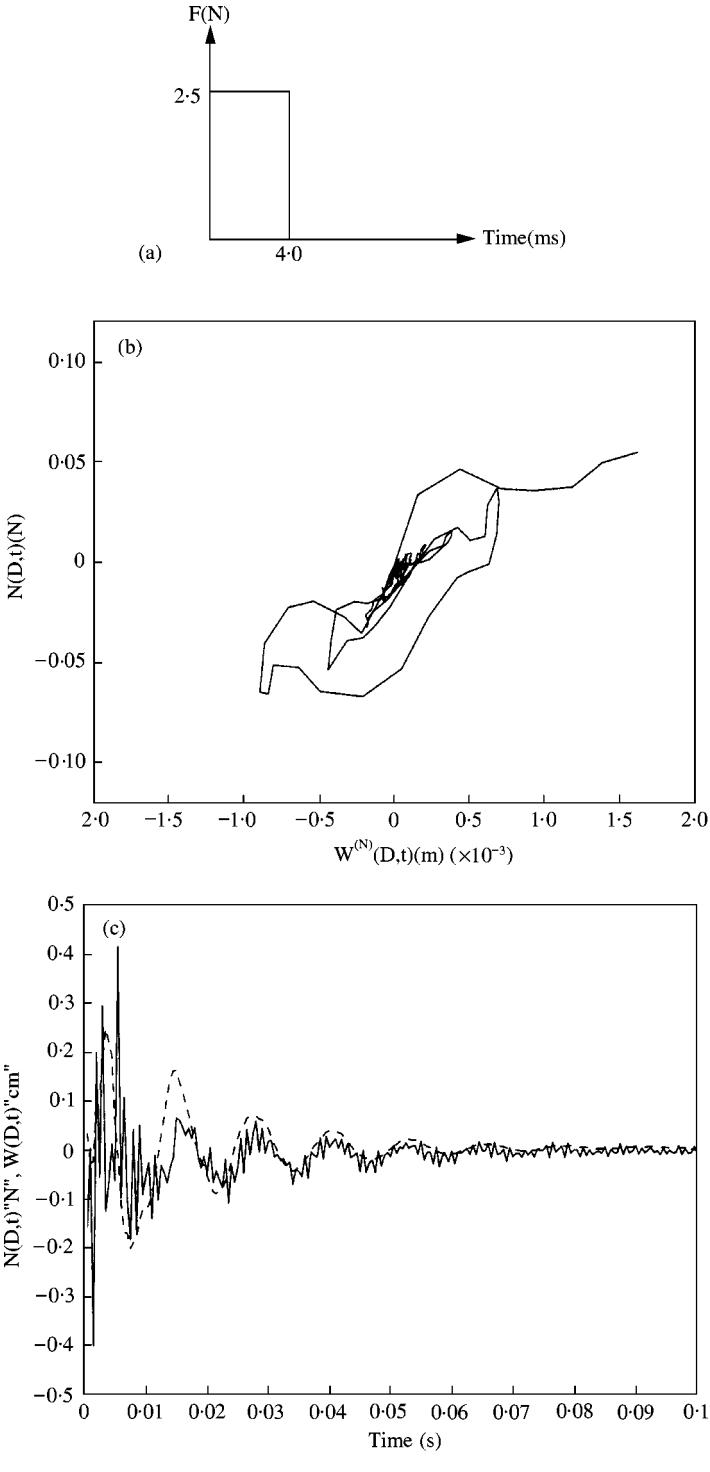

Figure 21. Transient response of beam S-Ia to a rectangular input pulse of 2·5 lb over 4·0 ms. (a) Applied transient force. (b) Plot of computed joint force versus joint transverse displacement. (c) Plot of computed joint force (——) and joint transverse displacement (- - - - -) versus time.

model of the bolted structure to compare with the uniform Structure I. In addition, this type of joint modelling is applicable to the study of micro/macroslip at the joint, as well as of the relative beam rotations. However, it is anticipated that such a methodology is not of such wide applicability as the one presented herein.

(4) Modelling of non-linear axial deformation effects in the bolted beams due to midplane stretching and non-linear axial inertia during transverse vibration. Again, this type of analysis can be used to study the relative slip between the two beams in the neighborhood of the joint, but the resulting model is not expected to have wide applicability to structures with more complex configurations.

ACKNOWLEDGMENTS

This work is supported by a Research Grant from the Department of Energy through Sandia National Laboratories. The authors would like to thank Dr. Daniel Segalman and Dr. Jeffrey Dohner for interesting and helpful discussions on many aspects of this work.

REFERENCES

1. M. GROPER 1985 *Experimental Mechanics* **25**, 172–174. Microslip and macroslip in bolted joint.
2. L. E. GOODMAN and J. H. KLUMPP 1956 *Journal of Applied Mechanics* **50**, 421–429. Analysis of slip damping with reference to turbine-blade vibration.
3. C. F. BEARDS 1983 *Journal of Vibration, Acoustics, Stress, and Reliability in Design* **105**, 369–373. The damping of structural vibration by controlled interfacial slip in joints.
4. B. F. FEENY and J. W. LIANG 1996 *Journal of Sound and Vibration* **195**, 149–154. A decrement method for the simultaneous estimation of Coulomb and viscous friction.
5. A. FERRI and B. S. HECK 1998 *Journal of Vibration and Acoustics* **120**, 588–595. Vibration analysis of dry friction damped turbine blades using singular perturbation theory.
6. M. B. KARAMIS and B. SELCUK 1993 *Wear* **166**, 73–83. Analysis of the friction behaviour of bolted joints.
7. K. K. PADMANABHAN and A. S. R. MURRY 1991 *Proceedings of Institution of Mechanical Engineers* **205**, 121–129. Damping in structural joints subjected to tangential loads.
8. K. K. PADMANABHAN 1992 *International Journal of Mechanical Tools Manufacture* **32**, 305–314. Prediction of damping in machined joints.
9. G. SHI and S. N. ATLURI 1992 *American Institute of Aeronautics and Astronautics Journal* **30**, 234–240. Nonlinear dynamic response of frame-type structures with hysteretic damping at the joints.
10. Y. S. SHIN, J. C. IVERSON and K. S. KIM 1991 *Journal of Pressure Vessel Technology* **113**, 402–408. Experimental studies on damping characteristics of bolted joints for plates and shells.
11. S. VITELLESCHI and L. C. SCHMIDT 1977 *Journal of the Structural Division* **103**, 1447–1460. Damping in friction-grip bolted joints.
12. E. F. CRAWLEY and A. C. AUBERT 1986 *American Institute of Aeronautics and Astronautics Journal* **24**, 155–162. Identification of nonlinear structural elements by force-state mapping.
13. Y. REN and C. F. BEARDS 1998 *Journal of Vibration and Acoustics* **120**, 331–338. Identification of 'effective' linear joints using coupling and joint identification techniques.
14. Y. REN, T. M. LIM and M. K. LIM 1988 *Journal of Vibration and Acoustics* **120**, 324–330. Identification of properties of nonlinear joints using dynamic test data.
15. R. H. B. FEY, D. H. VAN CAMPEN and A. DE KRAKER 1996 *Journal of Vibration and Acoustics* **118**, 147–152. Long term structural dynamics of mechanical systems with local nonlinearities.
16. L. GAUL 1985 *American Society of Mechanical Engineers Design Engineering Division Conference and Exhibit on Mechanical Vibration and Noise, Cincinnati, OH*, September 10–13, 1985, 1–8. Analytical and experimental study of the dynamics of structures with joints and attached substructures.
17. H. S. TZOU 1990 *Journal of Sound and Vibration* **143**, 407–422. Non-linear joint dynamics and controls of jointed flexible structures with active and viscoelastic joint actuators.
18. E. E. UNGAR 1973 *Journal of Sound and Vibration* **26**, 141–154. The status of engineering knowledge concerning the damping of built-up structures.